yield 120 mg (yield 63%) of (S)-3·HCl: mp 257–258 °C [$[\alpha]^{25}_{578}$ +64.5 (c 0.11, MeOH)]; mass spectrum, m/e 279 (M^+). Anal. ($C_{19}H_{21}NO·HCl·H_2O$) C, H. (R)-3·HCl was obtained as described above from (R)-10·HCl, in a yield of 63%, mp 257–258 °C [$[\alpha]^{25}_{578}$ −64.0 (c 0.289, MeOH)].[20]

Determinations of Enantiomeric Purity. The enantiomeric excess of (R)-3 and (S)-3 was determined as follows: 10-mg samples of (R)-3 and (S)-3 were treated with 4 μL of triethylamine and extracted from ether. Each extract was evaporated to dryness with N_2 and allowed to react with triethylamine (1 μL) and (S)-(−)-α-methylbenzyl isocyanate (5 μL, Aldrich Chemical Co, Milwaukee, WI) for 5 h at room temperature. A sample of the reactive mixture was evaporated under a stream of N_2 and redissolved in 100 μL of mobile phase [0.05 M KH_2PO_4 containing 35% (w/v) CH_3CN, pH 3.0]. HPLC chromatographic separations were carried out with the mobile phase just described, and 0.2 μg of the derived carbamate was injected. The results of HPLC analyses showed that the diastereomeric excess of (S,R)-11 and (S,S)-11 were greater than 99%.

Acknowledgment. This work was supported by USPHS grants NS-15439 (J.L.N.) and MH-47370 and MH-34006 (R.J.B.). We also thank Dr. Peter Lampen for the determination of enantiomeric purity.

Registry No. (S)-3, 114033-64-6; (S)-3·HCl, 113725-41-0; (R)-3, 88247-21-6; (R)-3·HCl, 114033-65-7; 6, 53055-08-6; 7, 53626-57-6; (±)-8, 114033-59-9; (±)-9, 114033-60-2; (±)-10, 113725-39-6; (±)-10·HI, 114033-61-3; (S)-10·HCl, 113678-77-6; (S)-10·dibenzoyl-L-tartrate, 114033-63-5; (R)-10·HCl, 83207-98-1; (SS)-11, 114033-67-9; (SR)-11, 114033-66-8; C_3H_7I, 107-08-4; (S)-$C_6H_5CH(CH_3)NCO$, 14649-03-7.

The Hypothetical Active Site Lattice. An Approach to Modelling Active Sites from Data on Inhibitor Molecules

Arthur M. Doweyko

Uniroyal Chemical Co., Inc., World Headquarters, Middlebury, Connecticut 06749. *Received November 5, 1987*

Microcomputer-assisted methods are described that allow the mathematical construction of a hypothetical active site lattice (HASL) which can model enzyme–inhibitor interactions and provides predictive structure–activity relationships for a set of competitive inhibitors. The inhibitor set can be structurally dissimilar, including acyclic and cyclic moieties normally refractory to classical parameter-based quantitative structure–activity relationship strategies. With use of three-dimensional Cartesian coordinates representing energy-minimized inhibitor conformations, a four-dimensional space-filling description is generated, wherein the fourth dimension can be a user-selected physiochemical property such as hydrophobicity or electron density. The multidimensional lattices thus generated are used to quantitatively compare molecules to one another. Composite lattices of more than one molecule are merged with binding data to form a HASL capable of predicting inhibitor binding and relative orientation. Details of the algorithms and assumptions utilized are illustrated for competitive inhibitors of yeast glyoxalase-I and *E. coli* dihydrofolate reductase.

Computer-assisted drug design is a constantly evolving area of inquiry that presently encompasses many distinctly unique approaches.[1-6] Some of these methods provide insight to active-site or receptor-binding requirements and include statistical techniques that yield quantitative relationships between structure and activity (QSAR) through the use of substituent-related physiochemical parameters,[7] pattern recognition techniques designed to classify bioactive compounds according to pharmacophores,[8-10] and discriminant analysis with fragment molecular connectivity to classify drugs.[11] In addition, considerable effort has been expended to relate bioactivity to molecular shape[12] or to occupied space by utilizing distance geometry methods that consider molecular conformational flexibility.[13] Although these methods represent powerful tools that provide insight to active site shape and binding requirements, they are necessarily biased since the results are based on arbitrarily chosen molecular overlays or binding-site points.

In the present investigation, a novel approach was formulated relying on a computer-assisted molecule to molecule match, which makes use of a multidimensional representation of inhibitor molecules. Furthermore, the results of such matching are used to construct a hypothetical active site by means of a lattice of points which is capable of modelling enzyme–inhibitor interactions. This technique is referred to herein as HASL.

Specifically, portions of the space occupied by an individual molecule are assigned parameter values corresponding to the physiochemical nature of the atom in that space. It is through such molecular four-dimensional (4D) representations that it becomes possible to quantify comparisons between different molecules. The information from selected structures is merged to yield a composite lattice of points (the HASL) which effectively captures the shape and binding properties of an active site. Quantitative predictions of inhibitor binding are obtained by means of computer-assisted fitting of molecules into the HASL. The power of the HASL approach is illustrated herein by the generation of enzyme/inhibitor models for yeast glyoxalase-I and *E. coli* dihydrofolate reductase.

Methods

Since the methods developed for the construction and use of a HASL are unique and somewhat complex, they will be presented in a stepwise format with appropriate

(1) Gund, P. *X-Ray Crystallogr. Drug Action* (Course Int. Sch. Crystallogr., 9th, 1983, publ. 1984), p 495.
(2) Hopfinger, A. J. *Pharm. Int.* **1984**, *5*(9), 224.
(3) Marshall, G. R. *Comput.-Aided Mol. Des.* **1984**, 1.
(4) Jurs, P. C.; Stouch, T. R.; Czerwinski, M.; Narvaez, J. N. *J. Chem. Inf. Comput. Sci.* **1985**, *25*, 296.
(5) Hopfinger, A. J. *J. Med. Chem.* **1985**, *28*(9), 1133.
(6) Bowen-Jenkins, P. *Lab. Pract.* **1985**, *34*, 10.
(7) Silipo, C.; Hansch, C. *J. Am. Chem. Soc.* **1975**, *97*, 6849.
(8) Cammarata, A.; Menon, G. K. *J. Med. Chem.* **1976**, *19*, 739.
(9) Menon, G. K.; Cammarata, A. *J. Pharm. Sci.* **1977**, *66*, 304.
(10) Jurs, P. C.; Isenhour, T. *Chemical Applications of Pattern Recognition*; Wiley-Interscience: New York, 1975.
(11) Henry, D. R.; Block, J. H. *J. Med. Chem.* **1979**, *22*, 465.
(12) Hopfinger, A. J. *J. Am. Chem. Soc.* **1980**, *102*, 7196.
(13) Crippen, G. M. *J. Med. Chem.* **1979**, *22*, 988.

0022-2623/88/1831-1396$01.50/0

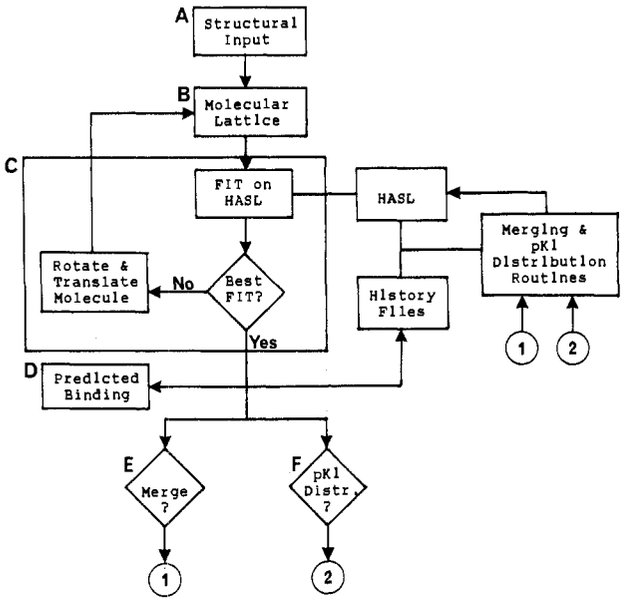

Figure 1. HASL logic flow. Step A: input of Cartesian Coordinates of energy-minimized structure. Step B: construction of lattice composed of orthogonal points in space found within the molecular van der Waal's radius and physiochemical descriptors. Step C: fitting routine involving superposition of molecular lattice on HASL. Step D: generation of results, which include binding prediction, record (HISTORY) files, and options to merge lattices and/or calculate partial pK_i distribution. Details of each step are discussed in the text.

references made to the logic flow chart in Figure 1.

Molecular Representation. A variety of methods are known for the representation of molecules in 3D space. These include the use of molecular shape descriptors,[14] steric mapping techniques,[15] and molecular volumes.[16-18] In order to minimize the number of calculations needed for 3D molecular manipulations, a computationally simple method was sought. This concern is particularly important when using desk-top microcomputers having limited speed, even when equipped with numeric coprocessors.

In the present study, the Cartesian coordinates of a molecule are obtained from an energy-minimization routine (step A, Figure 1) and these, in turn, are converted to a set of equidistant points arranged orthogonally to each other, separated by a distance that will be referred to as the resolution, and all lying within the van der Waal's radii of the atoms constituting the molecule. Such a framework of points will be referred to as a molecular lattice, and its construction corresponds to step B of Figure 1. This lattice has the distinct computational advantage of a limited number of points with the number dependent upon the size of molecule and resolution chosen.[17] The interrelationship of molecular size, resolution, and the number of lattice points will be discussed later.

Additional descriptive information can be made a part of the molecular lattice. For example, it is possible to construct a 4D lattice as illustrated in Figure 2. A portion of the molecule (panel 2A) is shaded to indicate atoms of different type (e.g., electron-rich, electron-poor). The conformation of the molecule is assumed to be energy-minimized. The superposition of atomic (van der Waal)

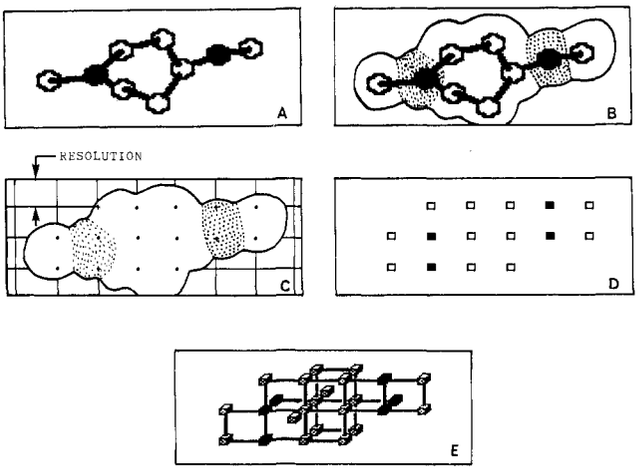

Figure 2. Schematic representation of 4D HASL construction: (A) energy-minimized molecular structure with black and white atomic characteristics, (B) superposition of van der Waal's molecular volume, (C) identifying molecular lattice points imbedded within the molecular lattice, (D) lattice points shown in two dimensions, (E) a three- and four-dimensional representation of these lattice points.

radii on the lattice is shown in panel 2B. The lattice points are developed on the basis of the resolution and result in an overlay of points that are imbedded within the molecular volume. This is illustrated in two dimensions in panel 2D. Included in the molecular lattice is additional information regarding the atomic character encountered at each point. The shaded lattice points reflect the presence of this fourth dimensional value. Panel 2E depicts a completed molecular lattice in three dimensions with connecting lines to help visualize depth. The fourth dimension in this example could be the electron density at occupied lattice points.

Fitting Routine. After conformational energy minimization, the comparison of one molecule with another can be carried out by first generating a 4D lattice of one molecule to act as a stationary reference. A second molecule is carried through the same routine, and its 4D lattice is compared to the reference. The degree of matching between the two molecules is based on the degree of correspondence between the points of the two lattices, i.e., on the number of points the two lattices have in common. A convenient measure of matching, or FIT, is given by eq 1, wherein FIT is the sum of the fraction of molecular

$$\text{FIT} = L(\text{common})/L(\text{ref}) + L(\text{common})/L(\text{molecule}) \quad (1)$$

lattice points and the fraction of reference lattice points found to be common. Thus, a perfect match of two molecular lattices would correspond to a FIT of 2. This procedure provides the fitting routine (step C, Figure 1) with a quick means of gauging the progress of molecular matching.

The fitting routine also involves a stepped progression of translational and rotational movements, with every step generating an intermediate lattice. A satisfactory search pattern for molecules having 20–40 atoms is obtained when translational increments are equal to the resolution (2–4 Å) and rotational increments are limited to 10–20 degrees about each of three axes. The molecule is carried through this series of movements, and FIT values are determined at each increment. The search pattern is considered completed when a maximum value of FIT has been reached. In this way, the comparison between two molecules is quantifiable, and their spatial orientations have been aligned with maximum correspondence. This is

(14) Meyer, A. Y. *J. Chem. Soc., Perkin Trans. II* **1985**, 1161.
(15) Motoc, I.; Marshall, G. R.; Labanowski, J. *Z. Naturforsch., A.: Phys. Chem., Kosmophys.* **1985**, *40A*, 1121.
(16) Connolly, M. L. *J. Am. Chem. Soc.* **1985**, *107*, 1118.
(17) Stouch, T. R.; Jurs, P. C. *J. Chem. Inf. Comput. Sci.* **1986**, *26*, 4.
(18) Richards, F. M. *Methods Enzymol.* **1985**, *115*, 440.

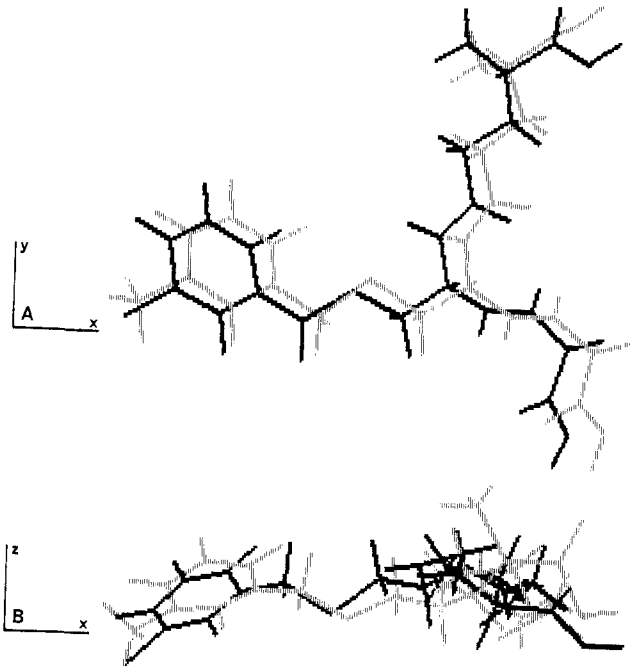

Figure 3. Superposition of G16 (black) and G17 (grey) carried out by using molecular lattices at a resolution of 4 Å.

possible since the 4D lattices contain atomic physiochemical character, which help lock together similar submolecular elements. A predicted binding constant, e.g., pK_i, is generated by the addition of partial pK_i values belonging to the common lattice points (step D, Figure 1). The origin of partial binding constants is discussed in the next section. Record files, referred to as HISTORY files, are also generated in order to keep track of which HASL points corresponded to a best FIT.

The outcome of such a fitting routine is illustrated in Figure 3 wherein two S-substituted glutathione analogues are compared, namely, *S*-[(3-methylphenyl)methyl]glutathione (**G16**) and *S*-[(3-chlorophenyl)methyl]glutathione (**G17**), portrayed in gray and black, respectively. The resolution chosen for this comparison was 3 Å. Panels 3A and 3B represent views of the superposed molecules from along the *z* axis and *y* axis, respectively, to illustrate the close structural correspondence obtainable even at a 3-Å resolution. The degree of matching was calculated for this pair by using eq 1: FIT = 1.43 where L(common) = 20 points, L(reference, 16) = 29 points and L(molecule, 17) = 27 points.

Merging Routine. The molecular lattice description is a geometric construction that represents the space and nature of the space occupied by a molecule. Enzyme inhibition data, commonly expressed as $I(50)$ or K_i, is associated with the molecular lattice in order to model the interactions between an inhibitor molecule and the eventual HASL construct. Restricting this technique to the consideration of competitive inhibitors was done in the present investigation in order to focus on active-site binding. However, in principle, this method would lend itself to applications involving less definitive binding as is often encountered in studies where only $I(50)$ values are available, in cases where unspecified binding to a receptor is studied, or where in vivo data (e.g., percent growth inhibition) are considered.

As is true of classical QSAR methodology, a convenient expression of activity was sought. In the case of enzyme inhibition, activity data is expressed in terms of $-\log K_i$ or pK_i. As a first approximation, the total pK_i of an inhibitor is evenly divided among its lattice points, e.g., if

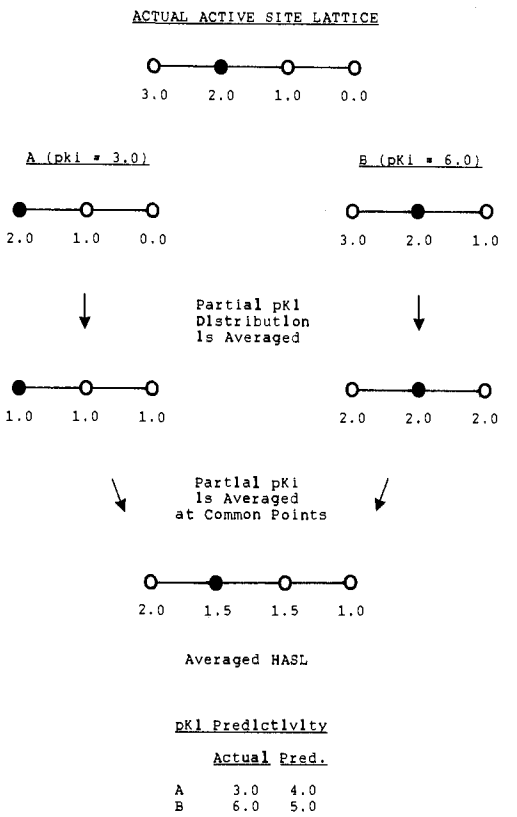

Figure 4. Partial pK_i estimates carried out by using an averaging method on the data for example molecules A and B. Partial pK_i values are listed below each lattice point.

a lattice contained 10 points, each point would bear $^1/_{10}$ of the total inhibitor pK_i. Although clearly simplistic, since partial pK_i distribution is made without regard to internal molecular heterogeneity, this procedure sets the stage for a separate redistributive process that is enacted when the binding data for a series of inhibitors is incorporated into a HASL.

After fitting the 4D lattice of a second molecule to the first, the information in both lattices is merged, resulting in a composite construct containing all the points present in either lattice (step E, Figure 1). The partial pK_i values associated with each lattice point are initially averaged. This simple averaging does not result in a exact solution to the partial pK_i distribution problem. That the real solution to this problem lies elsewhere is illustrated in Figures 4 and 5, wherein two molecules, A and B, having pK_i's of 3.00 and 6.00, respectively, are used to gain information about an active site depicted as a lattice consisting of four points with partial pK_i values of 3.00, 2.00, 1.00, and 0.00. This distribution of partial pK_i's can be considered as the lattice description that the inhibition data for molecules A and B needs to approach. As is evident in Figure 4, fitting of molecular lattices A and B to the HASL with averaged partial pK_i values yields poorly predicted molecular pK_i's. This result is particularly disturbing since A and B were used to construct the HASL, which, in turn, is incapable of predicting A or B pK_i accurately.

An alternate procedure was developed to estimate partial pK_i distribution among available lattice points (step F, Figure 1) and is shown in Figure 5. In this case, the averaged HASL of Figure 4 is used as a starting point. Fitting of molecule A to this HASL (step i, Figure 5) gives rise to a set of corrections referred to as IN and OUT, whose values are dependent on the overall error in predicted activity (referred to as ERROR). These corrections

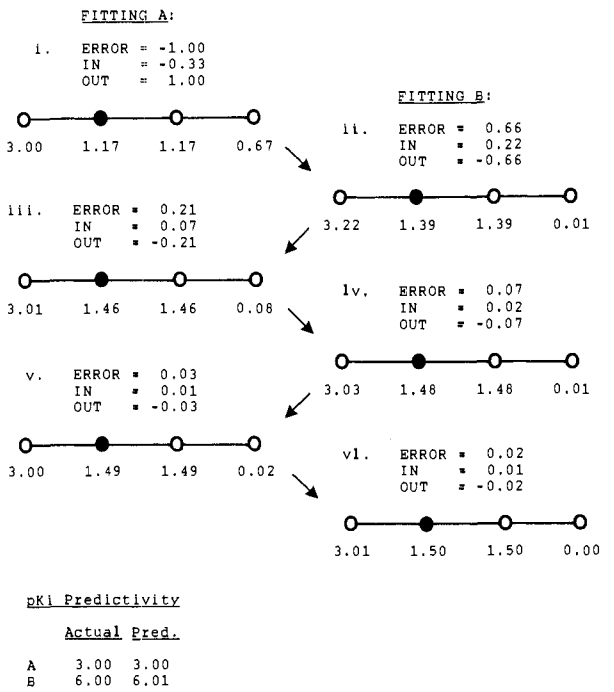

Figure 5. Partial pK_i estimates carried out by using an iterative method on the data for example molecules A and B. ERROR = actual pK_i - predicted pK_i. IN = correction calculated as ERROR/NI, where NI = number of lattice points in the overlap. OUT = correction calculated as -ERROR/NO, where NO = number of lattice points outside the overlap.

are determined as illustrated in the figure and are applied to the current partial pK_i values assigned to each HASL point. IN corrections are applied only to those points both A and the HASL have in common, while OUT corrections are made to HASL points not used. Step i illustrates this process where predicted pK_i ERROR = −1.00, IN = −0.33, and OUT = 1.00, giving rise to a corrected HASL (3.00, 1.17, 1.17, 0.67). The procedure is repeated with every molecule that was used to create the HASL and predictivity checked. A single iterative cycle would be considered as the fitting of both molecules A and B, each having been followed by appropriate corrections to the HASL description. The iterative cycle is repeated until an acceptable error in predictivity is achieved. In cases where the number of HASL points is small, the error in predictions is generally found to be minimized but not removed, since the available HASL points represent a limiting set of nodes into which partial pK_i values from a large number of molecules need to be placed. In the present A–B case, three iterative cycles (iterations i–vi) were found to result in a HASL with excellent predictivity.

Results and Discussion

Glyoxalase-I Inhibition. It was of interest to begin the investigation of the potential applications of a HASL by comparing the structures of a series of competitive enzyme inhibitors, which included cyclic and acyclic moieties. The enzyme system chosen for this purpose was yeast glyoxalase-I and a 41-member competitive inhibitor set was obtained from several sources.[19-24] As is shown in Table I, this set consists of S- and N-substituted and nor-*S*-glutathione analogues, a group of flavonoids, and flavonoid analogues. All structures were energy minimized by using MMPM(MM2) configured for use on an IBM-PC

Table I. Glyoxalase-I Inhibitor Set

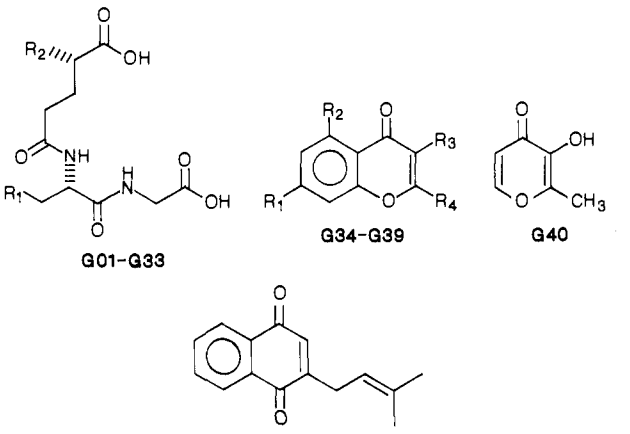

compd	R_1	R_2	pK_i[a]
G01	SCH_3	NH_2	2.38
G02	SCH_2CH_3	NH_2	3.32
G03	$S(CH_2)_2CH_3$	NH_2	4.03
G04	$S(CH_2)_3CH_3$	NH_2	4.55
G05	$S(CH_2)_4CH_3$	NH_2	4.56
G06	$S(CH_2)_5CH_3$	NH_2	4.80
G07	$S(CH_2)_6CH_3$	NH_2	4.98
G08	$S(CH_2)_7CH_3$	NH_2	5.00
G09	$SCH_2C_6H_5$	NH_2	4.03
G10	$SCH_2C_6H_4(4\text{-}OCH_3)$	NH_2	4.31
G11	$SCH_2C_6H_4(4\text{-}CH_3)$	NH_2	4.49
G12	$SCH_2C_6H_4(4\text{-}F)$	NH_2	4.52
G13	$SCH_2C_6H_4(4\text{-}Cl)$	NH_2	5.10
G14	$SCH_2C_6H_4(4\text{-}Br)$	NH_2	5.35
G15	$SCH_2C_6H_4(4\text{-}CN)$	NH_2	4.94
G16	$SCH_2C_6H_4(3\text{-}CH_3)$	NH_2	4.13
G17	$SCH_2C_6H_4(3\text{-}Cl)$	NH_2	4.68
G18	$SCH_2C_6H_4(2\text{-}Cl)$	NH_2	4.17
G19	$S(CH_2)_2C_6H_5$	NH_2	4.00
G20	$S(CH_2)_3C_6H_5$	NH_2	5.05
G21	$S(CH_2)_4C_6H_5$	NH_2	4.40
G22	$S(CH_2)_5C_6H_5$	NH_2	5.12
G23	$SCH_2COC_6H_5$	NH_2	3.71
G24	$SCH_2COC_6H_4(4\text{-}NH_2)$	NH_2	3.36
G25	$SCH_2COC_6H_4(4\text{-}OH)$	NH_2	3.71
G26	$SCH_2COC_6H_4(4\text{-}Cl)$	NH_2	4.29
G27	$SCH_2COC_6H_4(4\text{-}Br)$	NH_2	4.43
G28	$S(CH_2)_2COC_6H_5$	NH_2	4.41
G29	$SCH_2COC_6H_4(4\text{-}C_6H_5)$	NH_2	5.11
G30	$SCH_2C_6H_4(3\text{-}CF_3)$	NH_2	5.01
G31	$SCH_2C_6H_4(4\text{-}Br)$	$NHCOCH_3$	4.61
G32	$SCH_2C_6H_4(4\text{-}Br)$	H	3.57
G33	H	NH_2	3.02

compd	R_1	R_2	R_3	R_4	pK_i
G34	OH	H	OH	$3,4\text{-}(OH)_2C_6H_5$	4.88
G35	OH	OH	OH	$3,4\text{-}(OH)_2C_6H_5$	4.82
G36	OH	OH	OH	$2,4\text{-}(OH)_2C_6H_5$	4.52
G37	OH	OH	H	C_6H_5	4.08
G38	OH	OH	$4\text{-}(OCH_3)C_6H_5$	$COOC_2H_5$	4.95
G39	OH	OH	2,3-dihydro-2-[(4-OH)-C_6H_5]		4.76
G40	maltol				3.65
G41	lapachol				4.43

[a] pK_i values were calculated from $I(50)$ data in ref 19 using the relationship: $K_i = [I(50) \times K_m]/(K_m + S)$ for compounds **G01–G28**. Other K_i data was obtained directly: **G29** (ref 20), **G30** and **G31** (ref 22), **G32** (ref 23), **G33** (ref 21), **G34–G41** (ref 24).

(19) Vince, R.; Daluge, S.; Wadd, W. B. *J. Med. Chem.* **1971**, *14*(5), 402.
(20) Davies, H. Ph.D. Dissertation, University Microfilms, Ann Arbor, MI, 1983.
(21) Cliffe, E. E.; Waley, S. G. *Biochem. J.* **1961**, *79*, 475.
(22) Al-Timari, A.; Douglas, K. T. *Biochim. Biophys. Acta* **1986**, *870*, 160.
(23) Vince, R.; Wolf, M.; Sanford, C. *J. Med. Chem.* **1973**, *16*, 951.
(24) Douglas, K. T.; Gohel, D. I.; Nadvi, I. N.; Quilter, A. J.; Seddon, A. P. *Biochim. Biophys. Acta* **1985**, *829*, 109.

Table II. HASL Type (*H*) Definitions

MM2[a]	*H*	atom	type	MM2	*H*	atom	type
1	0	C	sp^3 alkane	15	+1	S	sulfide
2	0	C	sp^2 alkene	16	−1	S^+	sulfonium
3	−1	C	sp^2 carbonyl	17	−1	S	sulfoxide
4	0	C	sp acetylene	18	−1	S	sulfone
5	0	H	hydrogen	19	0	Si	silane
6	+1	O	COH, COC	21	−1	H	OH, alcohol
7	+1	O	C=O carbonyl	22	0	C	cyclopropyl
8	+1	N	sp^3	23	−1	H	NH, amine
9	+1	N	sp^2	24	−1	H	COOH, carboxyl
10	+1	N	sp	25	+1	P	phosphine
11	+1	F	fluoride	26	−1	B	trigonal boron
12	+1	Cl	chloride	27	0	B	tetrahedral boron
13	+1	Br	bromide	28	−1	H	vinyl hydrogen
14	+1	I	iodide	37	+1	N	imine nitrogen

[a] MM2 types are defined in the QCPE documentation.[25]

Table III. HASL-Predicted pK_i Values for Glyoxalase-I Inhibitors Compared with Actual Values Listed in Ascending pK_i Order

compd	actual pK_i	predicted pK_i	error	compd	actual pK_i	predicted pK_i	error
G01	2.38	2.29	0.09	**G36**	4.52	4.63	0.11
G33	3.02	3.04	0.02	**G12**	4.52	4.72	0.20
G02	3.32	3.35	0.03	**G04**	4.55	4.49	0.06
G24	3.36	3.71	0.35	**G05**	4.56	4.40	0.16
G32	3.57	3.67	0.10	**G31**	4.61	4.56	0.05
G40	3.65	3.72	0.07	**G17**	4.68	4.74	0.06
G23	3.71	3.26	0.45	**G39**	4.76	4.77	0.01
G25	3.71	3.62	0.09	**G06**	4.80	4.77	0.03
G19	4.00	4.06	0.06	**G35**	4.81	4.84	0.03
G03	4.03	3.91	0.12	**G34**	4.88	4.80	0.08
G09	4.03	4.17	0.14	**G15**	4.94	5.07	0.13
G37	4.08	4.06	0.02	**G38**	4.95	5.05	0.10
G16	4.13	4.23	0.10	**G07**	4.98	5.19	0.21
G18	4.17	4.18	0.01	**G08**	5.00	5.18	0.18
G26	4.29	4.24	0.05	**G30**	5.01	4.99	0.02
G10	4.31	4.49	0.18	**G20**	5.05	5.00	0.05
G21	4.40	4.45	0.05	**G13**	5.10	5.22	0.12
G28	4.41	4.52	0.11	**G29**	5.11	5.20	0.09
G41	4.43	4.43	0.00	**G22**	5.12	5.16	0.04
G27	4.43	4.36	0.07	**G14**	5.35	5.40	0.05
G11	4.49	4.70	0.21			average error (r = 0.981)	0.10

compatible system.[25] Starting conformations are shown in the structure drawings of Table I. Limitations regarding the built-in MMPM(MM2) parameter set precluded the direct investigation of other intriguing structural types such as carbamoylated glutathiones,[20] the *cis*- and *trans*-S-phenethenylglutathiones,[26] and α-hydroxy thiol esters,[27] all of which are competitive inhibitors of glyoxalase-I.

In order to provide the lattices with a physiochemical fourth-dimensional descriptor, a simple indicator variable was adopted. This variable is referred to as *H*, the HASL type, and is loosely based on the quantitative assessment of hydrophobicity derived from a variety of atom types reported for dihydrofolate reductase inhibitors.[28] The values of *H* are integers equal to −1, 0, or +1, roughly corresponding to atoms with low, medium, or high electron density, respectively. These *H* values are defined by atom type in Table II. It is through such internal atom type designations that different structures can be overlaid with an equivalent electronic "sense", i.e., similar atomic characteristics of two molecules can be aligned in 3D space. The advantage of this procedure is that it forces molecular alignment toward a maximum complementarity of space and physiochemical character within that space. This electronic directionality plays a particularly significant role in locking together apparently dissimilar structures, e.g., the glutathione and flavonoid analogues of the present study.

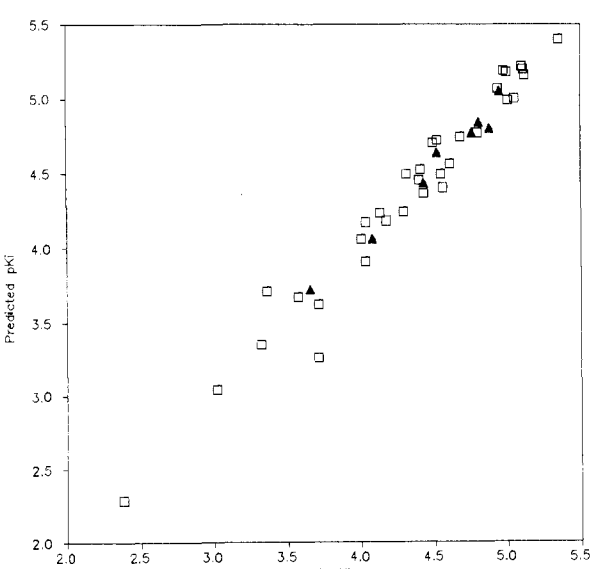

Figure 6. Comparison of HASL-predicted pK_i values with actual values for the glyoxalase-I inhibitor set. (□) Glutathione analogues (G01–G33), (▲) flavonoid analogues (G34–G41).

(25) MM2 (from QCPE) was adapted for use on the IBM-PC as MMPM by Kevin E. Gilbert and Joseph J. Gajewski.
(26) Creighton, D. J.; Weiner, A.; Buettner, L. *Biophys. Chem.* **1980**, *11*, 265.
(27) Hall, S. S.; Doweyko, L. M.; Doweyko, A. M.; Ryan-Zilenovski, J. S. *J. Med. Chem.* **1977**, *20*, 1239.
(28) Ghose, A. K.; Crippen, G. M. *J. Med. Chem.* **1985**, *28*, 333.

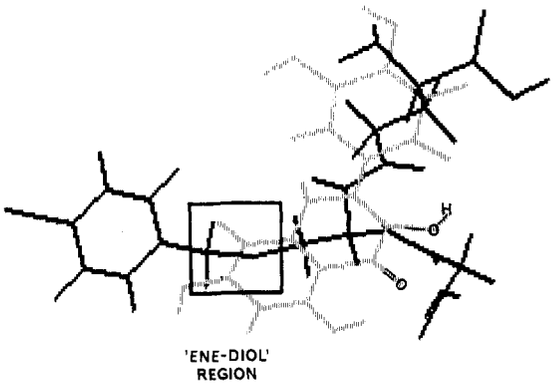

Figure 7. Superposition of G14 (black) and G35 (grey) through the independent fitting of each on the glyoxalase-I HASL at 3.0-Å resolution. The glyoxalase-I "ene–diol" reaction center is estimated to be near the thiomethyl portion of G14 (box). The corresponding "ene–diol" portion of **G35** is not located near the hypothetical reaction center.

With an arbitrary resolution of 3.0 Å and with *S*-methylglutathione (**G01**) as starting material, each of the 41 glyoxalase-I inhibitors was fitted and merged in turn to ultimately develop a HASL containing 88 lattice points. The inhibition data for each compound was then iteratively distributed among these points until the average error in prediction was less than 0.1 pK_i unit. A comparison of predicted and actual pK_i values for these inhibitors is presented in Table III and illustrated in Figure 6. It is important to note that this HASL represents a kind of composite map of an active-site binding pattern consistent with the structures and binding constants used. Thus, the action of docking each inhibitor into place within this model transcends traditional quantitative structure–activity relationships and provides a unique view of potential active site binding.

Inspection of the relative orientations of glutathione and flavonoid analogues after fitting into the HASL can provide suggestions regarding binding commonalities. To illustrate this point, such a comparison is made in Figure 7 with *S*-[(4-bromophenyl)methyl]glutathione (**G14**) and quercitin (**G35**). Flavonoids and other α-hydroxy carbonyl systems[27] have been considered as potential transition state analogue inhibitors of glyoxalase-I due to their structural and electronic similarities to the "ene–diol" transition state expected during the enzyme-catalyzed transformation of an α-keto hemimercaptal to an α-hydroxy thiol ester.[29] Despite the intuitively tempting analogy, quercitin, after docking to the glyoxalase-I HASL, does not appear to orient itself so that its "ene–diol" region is near the expected reaction center, i.e., thiobenzyl portion of **G14**. This observation would suggest that an alternative complementarity is possible wherein the "ene–diol" center of quercitin points out in the same direction as the polar glutathione backbone.

Dihydrofolate Reductase Inhibition

The preliminary studies conducted with glyoxalase-I inhibitors indicated that a HASL could be constructed with a variety of structural types. The mechanics of a model system were explored to a limited extent and found to yield reasonably predictive relationships. To further probe HASL capability, the dihydrofolate reductase (DHFR) system was chosen for study. A large number of DHFR inhibitors are known, which encompass a wide variety of structures. In addition, the crystal structure of the enzyme isolated from several sources is known, along with the active-site orientation of some of its most potent inhibitors, in particular, methotrexate (**D73**). The **D73** conformation at the active site of *E. coli* DHFR was obtained from the Brookhaven Protein Data Bank[30] and was used as a test probe of the HASL developed from other DHFR inhibitors.

The set of 72 inhibitors used to generate a DHFR HASL was taken from several sources[31-35] and is listed in Table IV. All structures were energy minimized by using MM2. An estimate of an appropriate resolution was made by examining the details of lattice construction from a single molecule representing the smallest structure from the 72 compound set, namely, 2,4-diamino-5-(methylphenyl)pyrimidine (**D01**). The effect of resolution on the number and nature of lattice points obtained is shown in Figure 8. The theoretical volumes of atoms in **D01**, having H = −1, 0, and +1, are 39, 449, and 101 Å^3 (as calculated from van der Waal radii), respectively. In terms of relative volume percent of each HASL type, this distribution is 6.6% of H = −1, 76% of H = 0, and 17% of H = +1. Discounting a slight discrepancy due to overlapping volumes, panel 8A indicates that these percentages are increasingly reflected in the lattice-point distribution as the point spacing decreases. However, as can be seen in panel 8B, decreasing values of resolution yield increasing numbers of lattice points. In an effort to minimize computation time and, in particular, the degrees of freedom associated with lattice points, a resolution value of 2.8 Å was considered optimal since it represents a value that is as large as possible while retaining a reasonably sensitive H distribution for the molecule, i.e., one that reflects the atomic makeup of the molecule.

In a manner analogous to classic QSAR, the DHFR inhibitor set was divided into two groups: a learning set and a test set. This was done in order to find out how well a HASL, which is known to be incomplete, could predict binding constants for molecules it has never seen. A learning set was selected from the 72 inhibitors by using parameters such as the number of different atoms, number of rings, and molecular weights in a repetitive version of the algorithm of Wooton et al.[36,37] The learning-set members chosen in this way are indicated with asterisks in Table IV and represent 37 compounds that differ from one another as much as possible in terms of the three parameters cited above.

The learning set was used to generate HASL descriptions at resolution values of 2.8, 3.2, 3.5, and 4.0 Å. The partial pK_i distribution problem for each HASL was solved to within a predictivity (predicted pK_i − actual pK_i) of 0.1 pK_i unit, with the exception of the 4.0-Å HASL, which could only be iteratively solved to a predictivity of 1.14 pK_i units. Each HASL was then fitted with the entire inhibitor

(29) Hall, S. S.; Doweyko, A. M.; Jordan, F. *J. Am. Chem. Soc.* **1978**, *100*, 5934.

(30) Bernstein, F. C.; Koetzle, T. F.; Williams, G. J. B.; Meyer, E. F., Jr.; Brice, M. D.; Rodgers, J. R.; Kennard, O.; Shimanouchi, T.; Tasumi, M. *J. Mol. Biol.* **1977**, *112*, 535.

(31) Hansch, C.; Li, R.; Blaney, J. M.; Langridge, R. *J. Med. Chem.* **1982**, *25*, 777.

(32) Muller, K. *Actual. Chim. Ther.* **1984**, *11*, 113.

(33) Coats, E. A.; Genther, C. S.; Selassie, C. D.; Strong, C. D.; Hansch, C. *J. Med. Chem.* **1985**, *28*, 1910.

(34) Burchall, J. J.; Hitchings, G. H. *Mol. Pharmacol.* **1965**, *1*, 126.

(35) Maag, H.; Locher, R.; Daly, J. J.; Kompis, I. *Helv. Chim. Acta* **1986**, *69*, 887.

(36) Wooton, R.; Cranfield, R.; Sheppey, G. C.; Goodford, P. J. *J. Med. Chem.* **1975**, *18*, 607.

(37) Doweyko, A. M.; Bell, A. R.; Minatelli, J. A.; Relyea, D. I. *J. Med. Chem.* **1983**, *26*, 475.

Table IV. Dihydrofolate Reductase Inhibitor Set

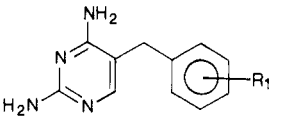

D01-D53

compd	R_1	pK_i[a]	compd	R_1	pK_i[a]
D01*	H	6.18	**D28**	4-$OCH_2CH_2OCH_3$	6.40
D02	3-F	6.23	**D29**	3-OH	6.47
D03	4-NH_2	6.30	**D30***	3-$OCH_2CH_2OCH_3$	6.53
D04	4-F	6.35	**D31**	3-$CH_2O(CH_2)_3CH_3$	6.55
D05	4-Cl	6.45	**D32**	3-OCH_2CONH_2	6.57
D06	3,4-$(OH)_2$	6.46	**D33**	3-CH_2OCH_3	6.59
D07*	4-CH_3	6.48	**D34**	4-$N(CH_3)_2$	6.78
D08	3-Cl	6.65	**D35**	3-$O(CH_2)_3CH_3$	6.82
D09	3-CH_3	6.70	**D36***	3-$O(CH_2)_5CH_3$	6.82
D10	4-Br	6.82	**D37**	4-$O(CH_2)_3CH_3$	6.89
D11	4-OCH_3	6.82	**D38***	3-$OCH_2C_6H_5$	6.99
D12*	4-$NHCOCH_3$	6.89	**D39***	3,4-$(OCH_2CH_2OCH_3)_2$	7.22
D13	3-OCH_3	6.93	**D40***	3,5-$(OCH_3)_2$-4-$O(CH_2)_2OCH_3$	8.35
D14	3-Br	6.96	**D41***	3,5-$(OCH_3)_2$-4-Br	9.22
D15	3-CF_3	7.02	**D42***	3,4-$(OCH_3)_2$-5-OCH_2COOH	8.59
D16*	3-I	7.23	**D43***	3-OCH_3-4-Br-5-OCH_2COOH	8.80
D17*	3-CF_3	7.69	**D44***	3,4-$(OCH_3)_2$-5-$O(CH_2)_2COOH$	9.43
D18*	3,4-$(OCH_3)_2$	7.72	**D45***	3-OCH_3-4-Br-5-$O(CH_2)_2COOH$	9.23
D19	3,5-$(OCH_3)_2$	8.38	**D46***	3,4-$(OCH_3)_2$-5-$O(CH_2)_3COOH$	10.46
D20*	3,4,5-$(OCH_3)_3$	8.87	**D47**	3-OCH_3-4-Br-5-$O(CH_2)_3COOH$	10.49
D21*	3,5-$(OH)_2$	3.04	**D48***	3,4-$(OCH_3)_2$-5-$O(CH_2)_4COOH$	10.18
D22*	4-$O(CH_2)_6CH_3$	5.60	**D49***	3-OCH_3-4-Br-5-$O(CH_2)_4COOH$	10.40
D23	4-$O(CH_2)_5CH_3$	6.07	**D50***	3,4-$(OCH_3)_2$-5-$O(CH_2)_5COOH$	10.62
D24	3-$O(CH_2)_7CH_3$	6.25	**D51**	3-OCH_3-4-Br-5-$O(CH_2)_5COOH$	10.92
D25	3-CH_2OH	6.28	**D52**	3,4-$(OCH_3)_2$-5-$O(CH_2)_6COOH$	10.30
D26	3,5-$(CH_2OH)_2$	6.31	**D53**	3-OCH_3-4-Br-5-$O(CH_2)_6COOH$	10.54
D27*	3-$O(CH_2)_6CH_3$	6.39			

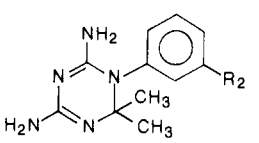

D54-D65

compd	R_2	pK_i	compd	R_2	pK_i	compd	R_2	pK_i
D54*	3-$CONH_2$	3.48	**D58**	3-Cl	5.87	**D62**	3-$(CH_2)_5CH_3$	5.75
D55*	3-CF_3	5.69	**D59***	3-I	5.58	**D63***	3-$C(CH_3)_3$	4.72
D56*	3-F	5.85	**D60***	3-CN	5.51	**D64**	3-$O(CH_2)_3CH_3$	6.02
D57*	H	4.51	**D61***	3-CH_3	5.42	**D65***	3-$OCH_2C_6H_5$	5.31

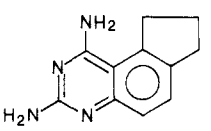

D66

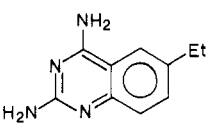

D67

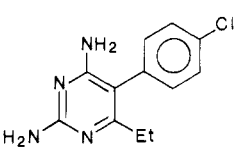

D68

compd	pK_i	compd	pK_i
D66*	8.36	**D68** (pyrimethamine)	6.55
D67*	7.17		

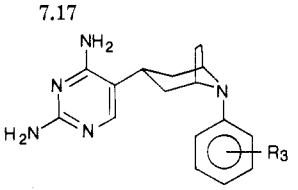

D69,70

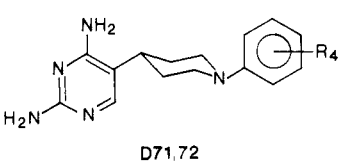

D71,72

compd	R_3	pK_i	compd	R_4	pK_i
D69*	3,5-$(OCH_3)_2$	9.31	**D71***	3,5-$(OCH_3)_2$	5.95
D70	4-OCH_3	8.30	**D72**	4-OCH_3	6.89

[a] Inhibition constants were obtained from the following references: **D01–D40** (ref 31), **D41–D53** (ref 32), **D54–D65** (ref 33), **D66** and **D67** (ref 34), **D68–D72** (ref 35). (*) Learning set member.

set of 72 compounds. The binding predictions obtained in this way are shown separately for the learning set and test set members in Figure 9. As might be expected, fair to good predictivity was obtained at all resolutions, with a perceptible scatter in evidence at 4.0 Å. Of particular interest are the predictivities found for the 35-member test set. In each case significantly more scattering was observed for the test set. Since the learning set HASL does not

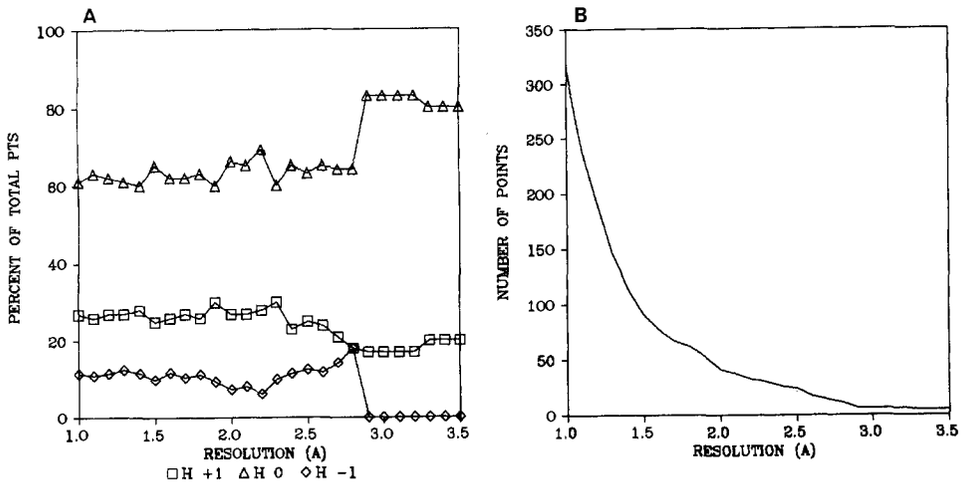

Figure 8. The effects of resolution choice on molecular lattice construction using **D01** as an example. (A) A plot of *H* distribution as a function of resolution indicates that *H*-distribution values level off at resolutions less than or equal to 2.8 Å. (B) A plot of the total number of lattice points as a function of resolution.

Table V. Partial Listing of the 140-Point DHFR HASL at 2.8-Å Resolution

point	*X*	*Y*	*Z*	*H*[a]	partial pK_i	*N*[b]
1	2.8	0.0	0.0	0	0.432	68
2	2.8	0.0	−2.8	0	0.613	21
3	0.0	0.0	0.0	0	0.327	60
4	0.0	0.0	2.8	0	−0.121	43
5	−2.8	0.0	0.0	0	0.367	56
6	−2.8	0.0	0.0	1	0.891	58
7	−2.8	2.8	2.8	1	1.147	22
8	−2.8	2.8	2.8	−1	0.103	12
9	−5.6	0.0	0.0	−1	0.081	16
10	5.6	0.0	−2.8	0	−0.037	17

[a] HASL type as defined in Table II. [b] *N* is the number of compounds providing data for a particular lattice point.

contain all the test-set structural information, the observed scatter is expected. The test set fitting results obtained at 2.8 Å are quite encouraging since the predicitivity is reasonable (correlation coefficient $r = 0.753$) and is superior to those obtained at higher resolution values. Despite the increase in degrees of freedom (i.e., the number of lattice points) at the lowest resolution, the 2.8-Å HASL appears to contain a real informational increase not present at higher resolutions.

On the basis of the preliminary study of the effect of resolution on HASL size and composition (Figure 8) coupled with the influence of resolution on predictivity (Figure 9), a resolution of 2.8 Å was chosen to develop the *E. coli* DHFR HASL with the entire 72 compound set. This was carried out by using the methods described, and the resulting HASL was found to contain 140 lattice points. A portion of this HASL is listed in Table V. Although it is difficult to draw any obvious structural insight from such a listing or its graphical representation, this matrix of points serves well to predict the binding of all 72 inhibitors used in its construction. With this HASL it is possible to compare the relative orientations of inhibitors after fitting is complete. In this way one can look for common modes of binding shared by these molecules.

The inhibitors selected for such a comparison were **D20**, **D51**, **D64**, and **D67**, representative of two pyrimidines, a triazine, and a quinazoline, respectively. Their relative orientations after fitting into the DHFR HASL are shown in Figure 10. Within the 2.8-Å resolution of this model, each inhibitor was positioned with its diamino ring system in roughly the same space. This would suggest that the diamino moiety binds in much the same way for each. It was also possible to examine this binding in detail by calculating the free energy, ΔG, attributable to binding of the diamino grouping, and in fact, to its components as well. Partial pK_i terms present at HASL points imbedded in one atom or group of atoms can be added and used in eq 2 to provide an estimate of ΔG per molecular fragment.

$$\Delta G_{\text{fragment-binding}} = (RT/2.303)\sum\text{partial p}K_i \quad (2)$$

This was done for the above inhibitors, and the results are listed in Table VI. Functional group contributions to binding were examined by Andrews et al. with a version of eq 2 applied to binding constant data for 200 compounds to generate a set of intrinsic binding energies.[38] The binding energy ranges reported for N and N^+ were 0.8–1.8 and 10.4–15.0 kcal/mol, respectively. The range observed for the inhibitor set of Table VI was 0–3.25 kcal/mol,

Table VI. Molecular Fragment Binding Energies (kcal/mol) Determined for Selected DHFR Inhibitors by Docking to the DHFR HASL

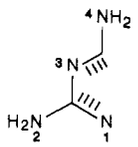

inhibitor	1-N	2-NH_2	3-N	4-NH_2
D20	1.97	0.10	0.69	1.25
D51	1.21	0.43	0.78	0.78
D64	1.08	0.47	1.21	0.00
D67	1.17	0.55	0.61	3.25
average	1.36	0.39	0.82	1.32

(38) Andrews, P. R.; Craik, D. J.; Martin, J. L. *J. Med. Chem.* **1984**, *27*, 1648.

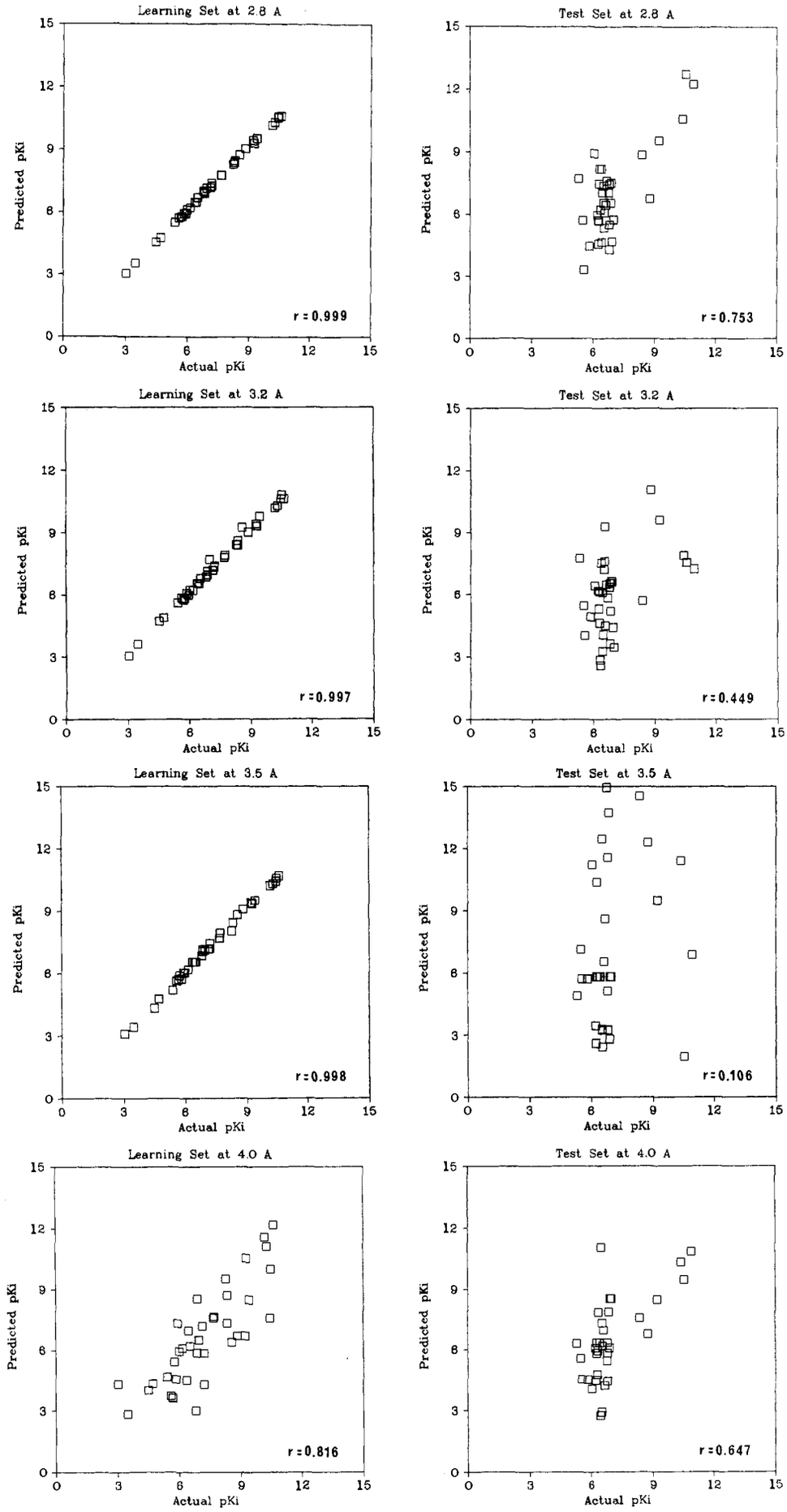

Figure 9. The effects of resolution choice on HASL predictivity using comparisons between learning and test set DHFR inhibitor data. Plots compare predictivities for both inhibitor sets at 2.8-, 3.2-, 3.5-, and 4.0-Å resolutions. Correlation coefficients (r) are indicated for each plot.

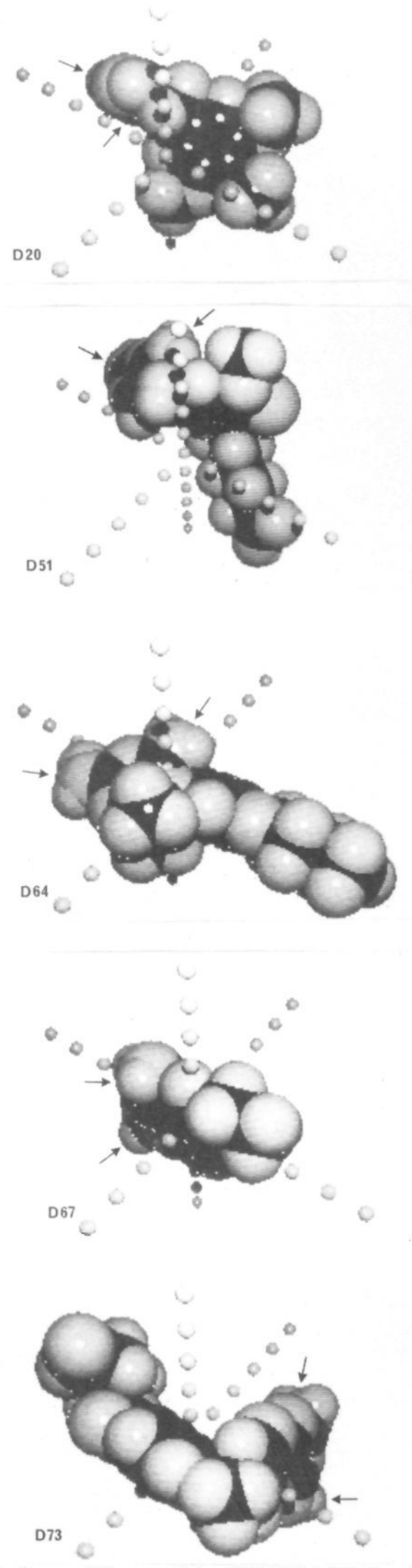

Figure 10. Space-filling models of DHFR inhibitors **D20**, **D51**, **D64**, **D67**, and **D73** showing orientation of each after fitting to the DHFR HASL. Axes are represented by small spheres set 2.0 Å apart. Arrows point to the location of the 2,4-diamino moiety common to each inhibitor.

consistent with an un-ionized mode of binding for the 2,4-diamino ring system.

DHFR was chosen for study because much is known about its active-site geometry and bound methotrexate (**D73**) conformation. In order to test how closely the DHFR HASL comes to mimicking the actual active site, **D73**, in its bound conformation, was used as a probe. Hydrogens missing from the X-ray coordinate data were added by using simple geometrical constraints. The orientation of **D73** in the DHFR HASL is also shown in Figure 10. With 65% of the HASL lattice points utilized, binding of **D73** was predicted as a pK_i of 10.11 (actual pK_i = 10.89). Considering that no methotrexate-like structures were used in this analysis, the predicted binding is in very good agreement with the actual value. The orientation of **D73** was found to be somewhat different from the other diamino systems examined. This observation is consistent with experimental data suggesting different active-site orientations for diaminopyrimidines and methotrexate.[39] Thus, by using the DHFR HASL, it was possible to model both the extent of binding and to suggest potential active site orientations for DHFR inhibitors.

Conclusions

A new and useful method of modelling active site–inhibitor interactions has been described. The method relies on the construction of a hypothetical active-site lattice (HASL) from inhibitor structure and binding affinities. Energy-minimized inhibitor conformations are utilized to build the model, and no initial assumptions are made regarding mode of binding. The mathematical fitting or docking of molecules by means of their molecular lattices to the HASL provides predictive data on their overall binding affinity and orientation. Furthermore, the method allows for the estimation of intrinsic fragmental binding energies.

The HASL can be realized at various resolutions. The choice of resolution was shown to influence predictivity. The method was found to be applicable to a variety of structurally diverse congeners, providing a means by which structure could be related to activity in cases not amenable to conventional QSAR analysis. In addition, the HASL was demonstrated to be a useful modelling tool through its prediction of affinity and orientation of an inhibitor as yet unassimilated.

Further enhancements to the HASL methodology are expected to include faster and more intelligent fitting algorithms (especially important for microcomputer applications), detailed exploration of the statistical consequences of resolution choice, incorporation of some structural flexibility paradigms to free inhibitor molecules from the static, energy-minimized assumption and the addition of algorithms to electronically synthesize potential inhibitors on the basis of the information content of a HASL. All programs are currently written in FORTRAN for use on IBM-PC compatible systems.

Registry No. **D01**, 7319-45-1; **D02**, 69945-57-9; **D03**, 69945-50-2; **D04**, 836-06-6; **D05**, 18588-43-7; **D06**, 71525-05-8; **D07**, 46726-70-9; **D08**, 69945-58-0; **D09**, 69945-56-8; **D10**, 69945-55-7; **D11**, 20285-70-5; **D12**, 69945-53-5; **D13**, 59481-28-6; **D14**, 69945-59-1; **D15**, 50823-94-4; **D16**, 30077-60-2; **D17**, 50823-94-4; **D18**, 5355-16-8; **D19**, 20344-69-8; **D20**, 738-70-5; **D21**, 80407-57-4; **D22**, 80407-60-9; **D23**, 80407-61-0; **D24**, 77113-60-1; **D25**, 77113-56-5; **D26**, 77113-54-3; **D27**, 80407-62-1; **D28**, 80407-59-6; **D29**, 77113-55-4; **D30**, 80416-29-1; **D31**, 77113-61-2; **D32**, 80407-58-5; **D33**, 77113-57-6; **D34**, 69945-51-3; **D35**, 77113-63-4; **D36**, 77113-62-3; **D37**, 77113-59-8; **D38**, 69945-60-4; **D39**, 73356-41-9; **D40**, 53808-87-0; **D41**, 56518-41-3; **D42**, 82830-22-6; **D43**, 93465-12-4; **D44**, 82830-23-7; **D45**, 93465-13-5; **D46**, 82830-24-8; **D47**, 91860-64-9; **D48**, 82830-25-9; **D49**, 91860-65-0;

(39) Champness, J. N.; Kuyper, L. F.; Beddell, C. R. In *Molecular Graphics and Drug Design*; Burger, A. S. V., Roberts, G. C. K., Tute, M. S., Eds.; Elsevier: New York, 1986.

D50, 82830-33-9; **D51**, 91860-66-1; **D52**, 82830-26-0; **D53**, 91860-67-2; **D54**, 70579-33-8; **D55**, 1492-81-5; **D56**, 3850-94-0; **D57**, 4022-58-6; **D58**, 13351-02-5; **D59**, 51012-14-7; **D60**, 70743-55-4; **D61**, 4038-60-2; **D62**, 70650-60-1; **D63**, 70579-36-1; **D64**, 70606-63-2; **D65**, 70579-38-3; **D66**, 7317-78-4; **D67**, 7319-46-2; **D68**, 58-14-0; **D69**, 94635-31-1; **D70**, 94635-30-0; **D71**, 94635-33-3; **D72**, 94635-32-2; **G01**, 2922-56-7; **G02**, 24425-52-3; **G03**, 24425-53-4; **G04**, 6803-16-3; **G05**, 24425-55-6; **G06**, 24425-56-7; **G07**, 24435-26-5; **G08**, 24435-27-6; **G09**, 6803-17-4; **G10**, 33812-35-0; **G11**, 33812-36-1; **G12**, 33812-37-2; **G13**, 6803-18-5; **G14**, 31702-37-1; **G15**, 33812-40-7; **G16**, 33812-41-8; **G17**, 33812-42-9; **G18**, 33812-44-1; **G19**, 33812-46-3; **G20**, 33812-47-4; **G21**, 33812-64-5; **G22**, 33812-48-5; **G23**, 33812-50-9; **G24**, 33812-51-0; **G25**, 33812-52-1; **G26**, 33812-53-2; **G27**, 33812-54-3; **G28**, 32728-47-5; **G29**, 114446-20-7; **G30**, 85261-24-1; **G31**, 114446-21-8; **G32**, 42583-87-9; **G33**, 70-18-8; **G34**, 528-48-3; **G35**, 117-39-5; **G36**, 480-16-0; **G37**, 480-40-0; **G38**, 15485-76-4; **G39**, 67604-48-2; **G40**, 118-71-8; **G41**, 84-79-7; DHFR, 9002-03-3; glyoxalase I, 9033-12-9.

Synthesis and Serotonin Receptor Affinities of a Series of Enantiomers of α-Methyltryptamines: Evidence for the Binding Conformation of Tryptamines at Serotonin 5-HT_{1B} Receptors

David E. Nichols,* David H. Lloyd, Michael P. Johnson, and Andrew J. Hoffman

Departments of Medicinal Chemistry and Pharmacognosy, and Pharmacology and Toxicology, School of Pharmacy and Pharmacal Sciences, Purdue University, West Lafayette, Indiana 47907. *Received November 16, 1987*

A procedure for the preparation of optically pure α-methyltryptamines (AMTs) from substituted indoles was developed. The key step in the sequence was the reductive amination of substituted indole-2-propanones with the commercially available pure enantiomers of α-methylbenzylamine, followed by the chromatographic separation of the resulting pair of diastereomeric amines by preparative centrifugal (Chromatotron) chromatography. Catalytic N-debenzylation then afforded the pure AMT enantiomers. Optical purity was established by chiral HPLC analysis of the 2-naphthoylamide derivatives. An improved procedure for the preparation of indole-2-propanones was also developed. To probe structure–activity relationships of serotonin receptors, affinities of the α-methyltryptamine enantiomers were then measured at the 5-HT_2 antagonist receptor subtype, with displacement of [^{3}H]ketanserin, and were estimated at the 5-HT_{1B} receptor, with displacement of [^{3}H]serotonin, respectively, in rat frontal cortex homogenates. Enantioselectivity at the receptor subtypes varied, depending on aromatic substituents. For a 5-hydroxy or 5-methoxy, the *S* enantiomer had higher affinity or was equipotent to the *R* enantiomer. This selectivity at [^{3}H]serotonin binding sites was reversed for 4-oxygenated α-methyltryptamines, where a 4-hydroxy or 4-methoxy did not enhance affinity over the unsubstituted compounds. These results can be explained, for the [^{3}H]serotonin displacement data, if the binding conformation is one where the ethylamine side chain is trans and lying in a plane perpendicular to the indole ring plane.

As part of our ongoing research into the mechanism of action of hallucinogens and other centrally active substances, it was of interest to prepare certain α-methyltryptamines (AMTs, **1a–f**) in an optically pure form. These compounds were designed to serve as chiral probes of serotonin (5-hydroxytryptamine) receptors. A general synthetic route was sought, such that several selected A-ring-substituted indoles might be transformed into the corresponding optically active AMTs. Another general concern was that reaction conditions be mild enough to allow the preparation of hydroxy-substituted AMTs as well, via their *O*-benzyl ethers.

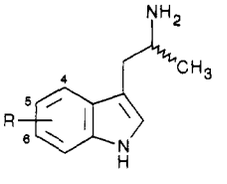

1a, R = H
b, R = 4-OCH_3
c, R = 5-OCH_3
d, R = 6-OCH_3
e, R = 4-OH
f, R = 5-OH

It has been hypothesized that 4- and 5-hydroxy-substituted tryptamines might bind to serotonin receptors in two different conformational extremes, such that the amine-to-oxygen distances in the two conformers would remain approximately the same.[1] It was anticipated that if this hypothesis were valid, a reversal of receptor stereoselectivity might be observed for binding of the enantiomers of 4- versus 5-hydroxy-substituted α-methyltryptamine.

This paper describes a general method for the synthesis of substituted α-methyltryptamine enantiomers. Ability of the isomers to displace [^{3}H]ketanserin and [^{3}H]serotonin from rat brain frontal cortex homogenates was then measured, as an indication of affinity for 5-HT_2 and 5-HT_{1B} receptors, respectively.

Chemistry

It was initially envisioned that a procedure analogous to that developed previously[2] for the preparation of optically pure substituted phenylisopropylamines from 1-phenyl-2-propanones could be employed, but with 1-indol-3-yl-2-propanones as the starting material. It fact, this procedure did work in principle, but it was accompanied by several serious problems. As a consequence, the approach was modified considerably, and this method is outlined in Scheme I.

Indole-2-propanones were prepared from the corresponding indolylnitropropanes (Scheme I). The alkoxyindoles **2a–d** used as starting materials either were purchased from commercial sources or were prepared from the appropriate *o*-nitrotoluenes by using our recently reported method.[3] Preparation of indole-2-propanone and 5-methoxyindole-2-propanone from the corresponding gramines has been reported by Heath-Brown and Phil-

(1) Nichols, D. E. *Proceedings, VIIIth Int. Symposium on Med. Chem., Vol. 2*; Swedish Pharmaceutical Press, Stockholm; 1985; p 103.

(2) Nichols, D. E.; Barfknecht, C. F.; Rusterholz, D. B.; Bennington, F.; Morin, R. D. *J. Med. Chem.* **1973**, *16*, 480.

(3) Lloyd, D. H.; Nichols, D. E. *J. Org. Chem.* **1986**, *51*, 4294.

(4) Heath-Brown, B.; Philpott, P. G. *J. Chem. Soc.* **1965**, 7165.

0022-2623/88/1831-1406$01.50/0